THE JOURNAL OF PHYSICAL CHEMISTRY B

ARTICLE

pubs.acs.org/JPCB

Prediction of the Temperature Dependence of the Surface Tension Of SO_2, N_2, O_2, and Ar by Monte Carlo Molecular Simulations

Jean-Claude Neyt,[†,‡] Aurélie Wender,[‡] Véronique Lachet,[‡] and Patrice Malfreyt*[,†]

[†]Clermont Université, Université Blaise Pascal, Laboratoire de Thermodynamique et Interactions Moléculaires, BP 10448, F-63000 Clermont-Ferrand, France

[‡]IFP Energies nouvelles, 1-4 avenue de Bois Préau, 92852 Rueil-Malmaison, France

ABSTRACT: We report Monte Carlo simulations of the liquid−vapor interface of SO_2, O_2, N_2, and Ar to reproduce the dependence of the surface tension with the temperature. Whereas the coexisting densities, critical temperature, density, and pressure are very well reproduced by the two-phase simulations showing the same accuracy as the calculations performed using the Gibbs ensemble Monte Carlo technique (GEMC), the performance of the prediction of the variation of the surface tension with the temperature depends on the magnitude of the electrostatic and repulsive−dispersive interactions. The surface tension of SO_2 is very well reproduced, whereas the prediction of this property is less satisfactory for O_2 and N_2, for which the average intermolecular electrostatic interactions are several orders smaller than the dispersion interactions. For argon, we observe significant deviations from experiments. The representation of the surface tension of argon in reduced units shows that our calculations are in line with the existing surface tensions of the Lennard-Jones fluid in the literature. This underlines the difficulty of reproducing the temperature dependence of the surface tension of argon with interactions only modeled by the Lennard-Jones pair potential.

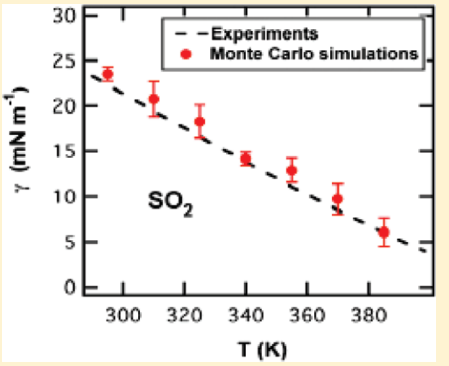

INTRODUCTION

Within the reduction of greenhouse gas emissions, large-scale CO_2 storage into underground formations like deep saline aquifers or depleted oil and gas fields is a promising option,[1] and scientific investigations have been particularly intense over the last years to develop optimized capture, transportation, and storage solutions.

Depending on the industrial sector (energy production, cement factory, refining), on the nature of fossil combustible used, and on the type of capture process involved, the composition of gases accompanying CO_2 (also called contaminant gases) can considerably vary on both qualitative and quantitative levels. Indeed, the CO_2 stream may account for different contaminant gases, such as N_2, O_2, Ar, SO_2, NOx, and H_2S, that can reach up to a few mol %. A detailed inventory of the nature and concentration of contaminants was proposed by Anheden et al. in 2004.[2] The impact of such gases on the phase equilibrium properties in the reservoir must be understood under geological storage conditions at high pressures and high temperatures.

Among other required properties, a good knowledge of gas [CO_2 + contaminants]−water interfacial tensions is needed for the design of storage projects. Indeed, CO_2 and contaminant gases may escape from the formation through different possible pathways, like abandoned wells, faults or fractures, or through the caprock, which is a low permeability media saturated with water that lies at the top of the reservoir. This risk of leakage through the caprock is largely governed by the fluid−fluid and the fluid−rock interfacial interactions. One of these interactions is the gas−water interfacial tension, which influences the flow process but also controls the capillary-sealing efficiency

$$P_c = P_{gas} - P_{water} = 2\gamma \cos(\theta)/R \quad (1)$$

where P_c is the capillary pressure in the saturated water caprock, γ is the gas−water interfacial tension, R is the largest connected pore throat in the caprock, and θ is the contact angle. Capillary breakthrough occurs when the overpressure, that is, the difference between the gas pressure in the reservoir and the water pressure in the caprock, exceeds the capillary pressure P_c.

The interfacial tension is thus a key property in assessing the suitability and the safety of acid gas storage sites. However, the experimental determination of this property under thermodynamic conditions close to the ones encountered in deep reservoirs is a difficult task. One possible solution is to use molecular simulation methods to predict the interfacial tension. The methodology for calculating the surface tension of liquid−vapor interfaces of pure molecular systems from a two-phase system is now robust, even though a certain number of factors such as the finite size effects,[3−6] the range of interactions,[7−10] the truncation effects,[7,11−13] the mechanical and thermodynamic definitions of the surface tension,[12,14,15] and the long-range corrections (LRCs) to the surface tension[9,11,12,15−17] can impact the calculated results for this property. Once the methodology was established, molecular simulations of the liquid−vapor interface showed a good reproduction of the temperature dependence of the surface

Received: May 2, 2011
Revised: June 28, 2011
Published: June 28, 2011

ACS Publications © 2011 American Chemical Society

tension for linear and branched alkanes,[9,11,12,18,19] cyclic and aromatic hydrocarbons,[20−22] water and acid gases,[15,23−26] and alcohols.[27] In the case of binary mixtures, the pressure dependence of the interfacial tension was successfully reproduced for methane−water,[28−30] CO_2−water,[31] and H_2S−water[31] binary mixtures under temperature and pressure conditions close to those encountered in geological storage. Recently, the dependence of the surface tension of water−alcohol mixtures on the alcohol concentration has also been reproduced by Monte Carlo simulations[32] using the TIP4P/2005[33] and the AUA4[34] models for water and alcohols, respectively.

Before investigating complex gas−water binary mixtures involving the presence of CO_2contaminant gases such as O_2, N_2, Ar, SO_2, we focus in a first stage on the temperature dependence of the liquid−vapor surface tension of these contaminants. The performance of the prediction from molecular simulations requires the development of transferable interaction potentials to model accurately the interactions between molecules. The potentials[35−38] used here have been developed from experimental liquid−vapor properties of the pure fluids such as saturated liquid densities, vapor pressures, and critical temperatures. In this context, the calculations reported here are purely predictive and demonstrate the transferability of the potential to predict the surface tension. However, the two-phase simulation methods are sensitive to the number of particles and to the equilibration times due to the fraction of molecules in the interfacial region and the inhomogeneity in density along the normal to the surface. The comparison of the coexisting densities and vapor pressures with those obtained with the GEMC technique[39,40] is essential for checking that the modeling of the slab geometry does not impact on the properties of the bulk liquid and vapor phases. Indeed, the GEMC technique is designed to accurately predict the coexisting densities by using two boxes, one for each coexisting phases. The advantage of the two-phase simulation is then the calculation of the interfacial properties.

In the Molecular Model of the Studied Gases section, we describe the potential models used for SO_2, O_2, N_2 and Ar and the computational procedures for the two-phase simulations. The different definitions of the surface tensions are presented in the Surface Tension section along with the operational expressions. We discuss in the Results and Discussion the different results of surface tensions and coexisting properties in relation with those obtained with GEMC methods. Finally, the Conclusions section provides a brief summary of our main results.

SIMULATION METHODOLOGY

Intermolecular Interactions. The total configurational energy U is defined by

$$U = U_{\mathrm{INTRA}} + U_{\mathrm{INTER}} + U_{\mathrm{LRC}} \tag{2}$$

where U_{INTRA}, U_{INTER}, and U_{LRC} are the intramolecular, intermolecular, and LRCs to the Lennard-Jones energy contributions, respectively. All SO_2, O_2, N_2, and Ar molecules are considered to be rigid, so $U_{\mathrm{INTRA}} = 0$.

The intermolecular interactions are composed of repulsion−dispersion and electrostatic contributions that are represented by Lennard-Jones (LJ) and Coulombic (ELEC) potentials, respectively

$$U_{\mathrm{INTER}} = U_{\mathrm{LJ}} + U_{\mathrm{ELEC}} \tag{3}$$

Table 1. Lennard-Jones Well Depth ε and Size σ, Partial Charges q, and Geometry of Sulfur Dioxide, Nitrogen, Oxygen, and Argon[a]

atom	ε/k_B (K)	σ (Å)	charge (e)
	SO_2 model[38]		
S	126.08	3.583	
O	46.41	2.990	−0.414
q^+			0.828
q^+−S distance (Å)		0.312	
S−O bond length (Å)		1.434	
O−S−O angle (deg)		119.3	
	O_2 model[37]		
O	43.183	3.1062	
q^+			4.200
q^-			2.100
O−O bond length (Å)		0.970	
O−q^- distance (Å)		0.485	
q^+−q^- distance (Å)		0.2	
	N_2 model[35]		
N	36.0	3.30	−0.5075
q^+			1.015
N−N bond length (Å)		1.098	
N−q^+ distance (Å)		0.549	
	Ar model[36]		
Ar	113.79	3.3952	

[a] k_B is the Boltzmann's constant.

The parameters of the repulsion−dispersion interactions are given in Table 1.

$$U_{\mathrm{LJ}} = \sum_{i=1}^{N-1}\sum_{j>i}^{N}\sum_{a=1}^{N_i}\sum_{b=1}^{N_j} u_{\mathrm{LJ}}(r_{iajb}) = \sum_{i=1}^{N-1}\sum_{j>i}^{N}\sum_{a=1}^{N_i}\sum_{b=1}^{N_j} 4\varepsilon_{ab}\left[\left(\frac{\sigma_{ab}}{r_{iajb}}\right)^{12} - \left(\frac{\sigma_{ab}}{r_{iajb}}\right)^{6}\right] \tag{4}$$

where r_{iajb} is the distance between force center a in molecule i and force center b in molecule j, ε_{ab} is the energy parameter of the interaction, and σ_{ab} is the Lennard-Jones core diameter. N_i is the number of force centers in the molecule i. The LJ parameters for the interactions between unlike sites were calculated using the Lorentz−Berthelot combining rules

$$\varepsilon_{ab} = (\varepsilon_{aa}\varepsilon_{bb})^{1/2} \quad \sigma_{ab} = \frac{1}{2}(\sigma_{aa} + \sigma_{bb}) \tag{5}$$

The electrostatic interactions were calculated using the Ewald sum method[23,41−43] from

$$U_{\mathrm{ELEC}} = \frac{1}{2\varepsilon_o V}\sum_{k\neq 0} Q(h)S(\mathbf{h})S(-\mathbf{h}) + \frac{1}{8\pi\varepsilon_o}\sum_i\sum_a\sum_{j\neq i} q_{ia}\sum_b q_{jb}\, erfc(\alpha r_{iajb})/r_{iajb} - \frac{\alpha}{4\pi^{3/2}\varepsilon_o}\sum_i\sum_a q_{ia}^2 - \frac{1}{8\pi\varepsilon_o}\sum_i\sum_a\sum_{b\neq a}\frac{q_{ia}q_{ib}}{r_{iaib}}\, erf(\alpha r_{iaib}) \tag{6}$$

where erfc(x) is the complementary error function and erf(x) is the error function. α is chosen so that only interaction pairs in the central cell need to be considered in evaluating the second term in eq 6. The functions $S(\mathbf{h})$ and $Q(h)$ are defined using eqs 7 and 8, respectively

$$S(\mathbf{h}) = \sum_i \sum_a q_{ia} \exp(i\mathbf{h}\cdot\mathbf{r}_{ia}) \tag{7}$$

$$Q(h) = \frac{1}{h^2} \exp\left(-\frac{h^2}{4\alpha^2}\right) \tag{8}$$

where the reciprocal lattice vector $\mathbf{h}$ is defined as $\mathbf{h} = 2\pi(l/L_x\mathbf{u}, m/L_y\mathbf{v}, n/L_z\mathbf{w})$ where $\mathbf{u}$, $\mathbf{v}$, and $\mathbf{w}$ are the reciprocal space basis vectors and l, m, and n take values of 0, ±1, ±2, ...±∞. The reciprocal space sum is truncated at an ellipsoidal boundary at the vector $|\mathbf{h}^{max}|$. The convergence factor α is calculated from $2\pi/L_x$. The maximum reciprocal lattice vectors parallel to the surface $|\mathbf{h}_x^{max}|$ and $|\mathbf{h}_y^{max}|$ were fixed to 8 and $|\mathbf{h}_z^{max}|$ to 40, respectively. The increase in $|\mathbf{h}_z^{max}|$ is required to account accurately for the long-range electrostatic interactions in the direction normal to the interface due to a larger dimension box in this direction. Because the systems studied here do not involve any electrostatic intramolecular interactions, the last term of eq 6 vanishes.

Molecular Model of the Studied Gases. The interaction potential of SO_2 consists of three Lennard-Jones centers located on the atoms of the SO_2 molecule and three electrostatic charges. Two negative charges q_O are located on oxygen atomic centers, and the positive charge q_+ (Figure 1a) is placed on the bisector of the OSO angle at distance d of 0.312 (Table 1) from the S atom. The S−O distance and the OSO angle are equal to 1.434 Å and 119.5°. This model[38] that accurately reproduces the experimental dipole moment of the molecule has been developed to perform calculations of the liquid−vapor phase envelope of pure SO_2.

The interaction potential of O_2 consists of two Lennard-Jones centers of forces separated by a distance of 0.970 Å. (See Table 1.) The positive charge q_+ is located in the center-of-mass of the molecule, and the negative charges q_- are 0.200 Å part on the O−O axis, as shown in Figure 1. This potential[37] developed by Boutard et al. is an adaptation of the Vrabec et al. potential.[36]

The N_2 model, developed by Delhommelle,[35] involves two Lennard-Jones centers with negative charges q_N with a bond length N−N distance of 1.098 Å. A positive charge q_+ is placed in the center-of-mass of the molecule. (See Table 1 and Figure 1.)

For argon, we used the potential model developed by Vrabec et al.[36] The Lennard-Jones parameters for argon are given in Table 1.

Long-Range Corrections to the Energy. Because the geometry of the system shows a heterogeneity along the axis normal to the interface (z axis), we calculated the LRC to the repulsion−dispersion energy as a function of z_k by splitting the cell into slabs of width δz. The total long-range correction energy U_{LRC} was then calculated by summing all of the local contributions of each slab. The U_{LRC} term was then added to the total energy of the system to be used in the Metropolis scheme. The long-range corrections to the total energy within each kth slab are defined by two parts[16]

$$U_{LRC} = \sum_{i=1}^{N_z} u_{lrc}(z_k) = \sum_{i=1}^{N_z} (u_{lrc}^{(1)}(z_k) + u_{lrc}^{(2)}(z_k)) \tag{9}$$

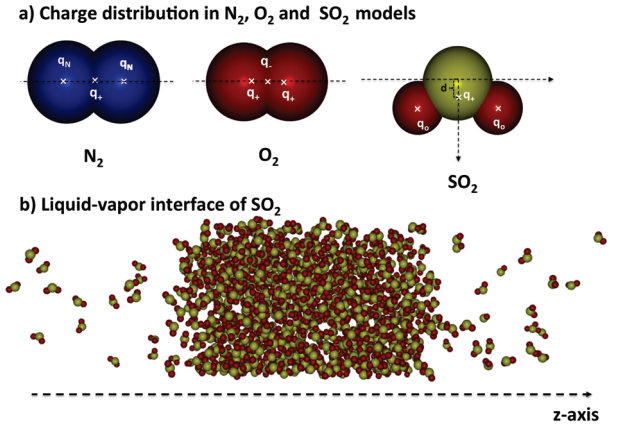

Figure 1. (a) Charge distributions in the N_2, O_2, and SO_2 gases and a configuration of the liquid−vapor interface of SO_2 at 344 K.

where N_z is the total number of slabs in the simulation box and

$$u_{lrc}^{(1)}(z_k) = \frac{8\pi}{3}\rho(z_k)^2 V_s \sum_{a=1}^{N_i}\sum_{b=1}^{N_j} \varepsilon_{ab}\left[1/3\left(\frac{\sigma_{ab}^{12}}{r_c^9}\right) - \left(\frac{\sigma_{ab}^{6}}{r_c^3}\right)\right] \tag{10}$$

$$u_{lrc}^{(2)}(z_k) = \pi\rho(z_k)V_s \int_{r_c}^{\infty} dr \int_{-r}^{r} d\Delta z \sum_{i=1}^{N_s} [\rho(z_{k+i}) - \rho(z_{k+i-1})]r\, U_{LJ,m}(r) \tag{11}$$

$\rho(z_k)$ and V_s are, respectively, the density and the volume of the slab k. Δz is defined as the difference $z - z_k$. N_s is the number of slabs between z and z_k. r_c is the cutoff radius fixed to 12 Å, and $U_{LJ,m}(r)$ is the intermolecular energy, with r being the distance between the two centers of mass of molecules i and j.

$$U_{LJ,m}(r) = \sum_a^{N_i}\sum_b^{N_j} 4\varepsilon_{ab}\left[\left(\frac{\sigma_{ab}}{r}\right)^{12} - \left(\frac{\sigma_{ab}}{r}\right)^{6}\right] \tag{12}$$

The first part of the LRC has an analytical form identical to the one associated with a homogeneous system but uses the local density $\rho(z_k)$ of the slab. The second part consists of a double integral that contains a series of density differences that renders this part cumbersome to calculate. As concerns the second part of the long-range corrections to the total configurational energy, it has been shown[9,16] that it represents only a minor contribution to the total long-range energy.

Computational Procedures. The simulation box was a rectangular parallelepipedic box of dimensions $L_x L_y L_z$ ($L_x = L_y$) with N molecules. The numbers of molecules are 850, 1400, 1150, and 2000 for the SO_2, O_2, N_2, and Ar gases. $L_x = L_y = 35$ Å for SO_2, N_2, and O_2, whereas for Ar, L_x and L_y were fixed to 40 Å. Periodic boundary conditions were applied in the three directions. MC simulations were performed in the *NVT* ensemble. Each cycle consisted of N randomly selected moves with fixed probabilities: translation of the center of mass of a random molecule and rotation of a randomly selected molecule around its center of mass. The frequency of each type of move depends on the molecule. For SO_2, N_2, and O_2 molecules, the occurrences of the various moves were 0.67 for translations and 0.33 for rotation. For argon, only the translation moves were considered.

The initial configuration was built by placing N molecules on the lattice points of a face-centered cubic structure. The

dx.doi.org/10.1021/jp204056d |J. Phys. Chem. B 2011, 115, 9421–9430

number N of molecules and the initial volume were chosen to build a dense bulk phase. The nodes of the lattice where molecules were placed as well as the orientation of these molecules were randomly chosen. MC simulations in the NpT ensemble were first performed on this bulk monophasic fluid configuration. The dimension of the resulting box was then increased along the z axis by placing two empty cells on both sides of the bulk dense liquid box.

An MC run consisted of 4×10^8 moves for the equilibration phase and additional 2×10^8 for the production phase. Because a cycle consists of N randomly selected MC moves, the number of cycles for each period is ~400 000 cycles for the equilibration and an additional 200 000 cycles for the production phase. Standard deviations of the ensemble averages were calculating by breaking the production runs into block averages. The magnitude of the standard deviations can depend on both the number of block averages and the number of cycles within each block. We must find a compromise among the convergence of the surface tension, relative small values of standard deviations, and a reasonable computational cost. To do so, we have represented in Figure A-1 the average surface tension of SO_2 as a function of the number of cycles within each block for the acquisition phase. This phase was broken into six blocks average of 35 000 MC cycles. We check that the surface tension of each block converges very well to the same value. This involves a standard deviation of ~0.8 mN m^{-1} for an average surface tension of 22 mN m^{-1}. The magnitude of this fluctuation can slightly depend on the temperature and the considered gas; it ranges from 0.8 to 1.9 mN m^{-1}.

One of the specificity of our MC methodology was the use of the LRCs to the configurational energy in the Metropolis scheme. The total LRC energy U_{LRC} was updated after each move of molecular position and was added to the energy of the system to be used in the Metropolis scheme. The cutoff radius for the truncation of the Lennard-Jones potential is fixed to 12 Å.

Surface Tension. The most commonly used methods[14,44−48] for the surface tension calculation are based on the mechanical route definition and use the tensorial components of the pressure. The first explicit form expresses the components of the pressure tensor as a function of the derivative of the intermolecular potential. This operational expression γ_{KB}, given by Kirkwood and Buff,[45] is given by

$$\gamma_{KB} = \frac{1}{2A}\left\langle \sum_{i=1}^{N-1}\sum_{j=i+1}^{N}\sum_{a=1}^{n_i}\sum_{b=1}^{n_j} \frac{\mathbf{r_{ij}}.\mathbf{r_{iajb}} - 3z_{ij}.z_{iajb}}{2r_{iajb}} \frac{dU(r_{iajb})}{dr_{iajb}} \right\rangle \quad (13)$$

where U is the total configurational energy defined in eq 2 and A is the surface area.

The definition of Irving and Kirkwood[46] γ_{IK} is based on the notion of the force across a unit area and takes advantage of expressing the local components of the pressure tensor along the direction normal to the surface. The surface tension is then expressed by

$$\gamma_{IK} = \frac{1}{2}\int_{-L_z/2}^{L_z/2} (p_N(z_k) - p_T(z_k))\, dz \quad (14)$$

where $p_N(z_k)$ and $p_T(z_k)$ are the normal and tangential components of the pressure tensor along the normal to the surface, respectively. The description of the calculation of the local components of the pressure tensor can be found elsewhere.[28,31]

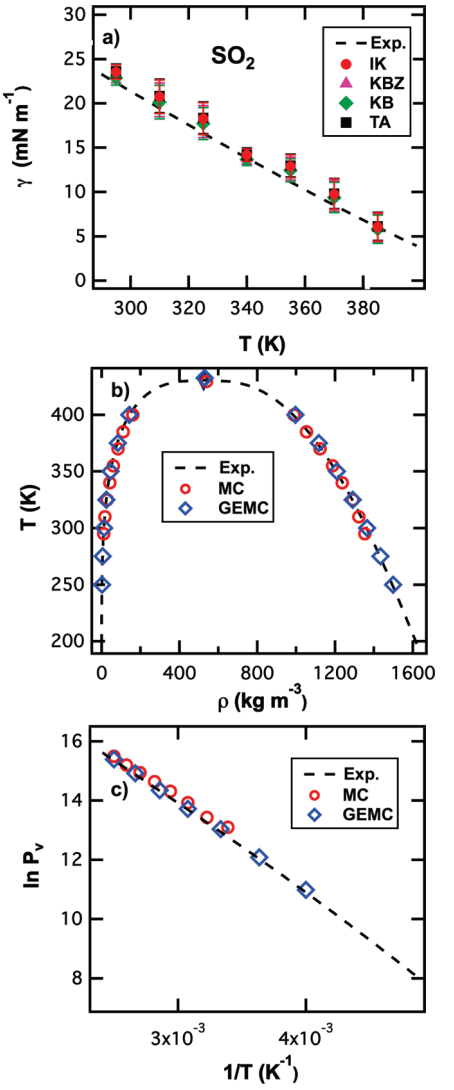

Figure 2. (a) Surface tension values of the SO_2 liquid−vapor interface as a function of temperature. (b) Liquid−vapor coexistence curve calculated from MC and GEMC methods. (c) Vapor pressure values as a function $1/T$. The experimental surface tensions are taken from ref 49, and the coexisting densities and vapor pressures are taken from ref 50.

A novel method based on the thermodynamic definition of the surface tension γ_{TA} has been recently established by Gloor et al.[14] and consists of perturbing the cross-sectional area of the system containing the interface. This infinitesimal change in the area is performed throughout a perturbation process for which the perturbed system (state $^{A+\Delta A}$) is obtained from an infinitesimal change ΔA of the area A of the reference system. The box dimensions $(L_x^{(A+\Delta A)}, L_y^{(A+\Delta A)}, L_z^{(A+\Delta A)})$ in the perturbed systems are changed using the following transformations $L_x^{(A+\Delta A)} = L_x^{(A)}(1+\xi)^{1/2}$, $L_y^{(A+\Delta A)} = L_y^{(A)}(1+\xi)^{1/2}$, and $L_z^{(A+\Delta A)} = L_z^{(A)}/(1+\xi)$ where $\xi \rightarrow 0$. The area $(A + \Delta A)$ of the perturbed state thus equals $L_x^{(A)}L_y^{(A)}(1+\xi)$, and ΔA is equal to $L_x^{(A)}L_y^{(A)}\xi$. The working expression is

$$\gamma_{TA} = \sum_k \lim_{\xi \rightarrow 0} -\frac{k_B T}{\Delta A} \times \ln\left\langle \exp\left(-\frac{(U^{(A+\Delta A)}(z_k, \mathbf{r}'^N) - U^{(A)}(z_k, \mathbf{r}^N))}{k_B T}\right)\right\rangle_{k,A} \quad (15)$$

dx.doi.org/10.1021/jp204056d |J. Phys. Chem. B 2011, 115, 9421–9430

Table 2. Surface Tension Values (mN m^{-1}) of the SO_2 Liquid−Vapor Interface at Different Temperatures[a]

	γ_{KB}		γ_{IK}		γ_{TA}		γ_{KBZ}			
T (K)	γ_{LRC}	γ	γ_{LRC}	γ	γ_{LRC}	γ	γ_{LRC}	γ	<γ>	γ_{exp}
					SO_2					
295	1.7_1	22.9_8	2.4_1	23.5_8	1.6_1	23.6_8	2.0_1	23.1_8	23.3_8	22.3
310	1.6_1	20.1_{19}	2.2_1	20.8_{19}	1.5_1	20.8_{19}	1.8_1	20.4_{19}	20.5_{19}	19.5
325	1.5_1	17.7_{18}	2.0_1	18.3_{18}	1.4_1	18.4_{18}	1.7_1	17.9_{18}	18.1_{18}	16.6
340	1.3_1	13.7_7	1.8_1	14.2_7	1.2_1	14.3_7	1.5_1	13.9_7	14.0_7	13.8
355	1.1_1	12.4_{13}	1.6_1	12.9_{13}	1.1_1	13.0_{13}	1.3_1	12.6_{13}	12.7_{13}	11.1
370	0.9_1	9.4_{17}	1.3_1	9.7_{17}	0.9_1	9.8_{17}	1.1_1	9.5_{17}	9.6_{17}	8.5
385	0.7_1	5.8_{16}	1.0_1	6.1_{16}	0.7_1	6.1_{16}	0.8_1	5.9_{16}	6.0_{16}	6.0
400	0.5_1	3.9_{15}	0.7_1	4.1_{15}	0.5_1	4.1_{15}	0.6_1	4.0_{15}	4.0_{15}	3.7

[a] Long-range corrections and the total surface tensions are given for each method. <γ> is averaged over the KB, IK, TA, and KBZ approaches. The experimental surface tensions are taken from ref 49. The long range corrections (γ_{LRC}) and the total surface tension (γ) are given for each method. The subscripts give the accuracy of the last decimal(s); that is, 22.9_8 means 22.9 ± 0.8.

$< \ldots >_{k,A}$ indicates that the average is carried out over the reference state and the k slabs. $U^{(A+\Delta A)}(z_k \mathbf{r}'^N)$ and $U^{(A)}(z_k \mathbf{r}^N)$ are the configurational energies of the slab k in the perturbed and reference states. We have also established a local version of the TA approach with specific LRCs.[12,15,19,22]

We have also developed a new operational expression of the surface tension based on the derivative of the potential with respect to the surface.[15] The working expression is referred to KBZ and corresponds to the local version of the KB expression.

$$\gamma_{KBZ} = \left\langle \frac{\partial U}{\partial A} \right\rangle_0 = \sum_k^{N_s} \left\langle \frac{\partial U_{z_k}}{\partial A} \right\rangle_0 = \sum_k^{N_s} \gamma_{KBZ}(z_k)$$
$$= \sum_k^{N_s} (\gamma_{KBZ}^{LJ}(z_k) + \gamma_{KBZ}^{ELE}(z_k)) \quad (16)$$

The reader is referred to refs 15, 28, and 31 for a review about the different derivations of these expressions. Because of the truncation of the Lennard-Jones potential, the surface tension must be corrected by specific LRCs. The operational expressions of these LRC contributions were also given in refs 15, 19, and 22 for the IK, KB, KBZ, and TA approaches.

RESULTS AND DISCUSSIONS

We start the discussion by the SO_2, O_2, and N_2 molecules because they involve the calculation of both electrostatic and repulsion−dispersion intermolecular interactions. We will finish this section by argon, for which only Lennard-Jones interactions were considered.

Figure 2a shows the temperature dependence of the surface tension of SO_2 calculated using the different definitions. The intrinsic and the LRC values of the surface tensions are reported in Table 2 with the experimental values.[49] First, the MC calculations show a quantitative prediction of the surface tension of SO_2 with average absolute deviations from experiments of 9, 6, 8, and 6% using the TA, KBZ, IK, and KB approaches. The different definitions give consistent values with respect to experiments, and the LRC part of the surface tension represents a contribution that increases from 10 to 15% with temperature. The decomposition of the SO_2 surface tension at 295 K into the Lennard-Jones, electrostatic, and LRC parts gives a positive LJ contribution of 10.5 mN m^{-1}, a positive electrostatic part of 9 mN m^{-1}, and a LRC contribution of 2.4 mN m^{-1}.

The equilibrium coexisting densities in the two-phase simulations were determined by fitting the equilibrium density profile to a hyperbolic tangent function of the form

$$\rho(z) = \frac{1}{2}(\rho_l + \rho_v) - \frac{1}{2}(\rho_l - \rho_v) \tanh\left(\frac{2(z - z_o)}{d}\right) \quad (17)$$

where ρ_l and ρ_v are the coexisting densities of the liquid and vapor phases, z_o is the position of the Gibbs dividing surface, and d is an approximate measure of the thickness of the interface. The liquid and vapor densities calculated from MC are reported in Figure 2b along with the densities calculated from GEMC[38] and the experimental ones.[50] The saturated liquid densities of SO_2 are predicted with an average absolute error of 1% for both MC and GEMC simulation methods.

Critical coordinates[51] (T_c and ρ_c) were estimated by fitting the simulated coexistence densities to the critical scaling law using an Ising-type critical exponent

$$\rho_l - \rho_v = B(T - T_c)^\beta \quad (18)$$

and to the law of rectilinear diameters

$$\frac{\rho_l + \rho_v}{2} = \rho_c + A(T - T_c) \quad (19)$$

where A and B are fitting parameters and $\beta = 0.325$ is an Ising-type critical exponent. The critical density and temperature are given in Table 5. The MC simulations predict $T_c = 429.4$ K and $\rho_c = 539.8$ kg m^{-3}, which are in excellent agreement with the experimental values with deviations from experiments of 0.3 and 3% for the temperature and density, respectively. The prediction is similar to that given by the GEMC simulations. In addition, we report in Figure 2c the Clausius−Clapeyron plot. The vapor pressure is calculated from averaging the diagonal elements of the pressure tensor over the slabs in the vapor phases. (See Figure B-1.) Typical profiles are shown in Figure B-2. The critical pressure is determined by a linear extrapolation of the Clausius−Clapeyron plot to the critical temperature ($T_c = 429.4$ K). We obtain $P_c = 8.5$ MPa against an experimental value of 7.9 MPa. The deviation from experiments is ∼7% and corresponds to that obtained from GEMC calculations.

The calculation of the surface tensions of oxygen show average deviations from experiments[52] of ∼15%, whatever the definition used. The values of the surface tensions are reported in Table 3 and in Figure 3a in the 90−110 K temperature range. At 90 K, for a surface tension of 14.6 mN m^{-1}, the contributions of the Lennard-Jones and the LRC are about 13.2 and 1.4 mN m^{-1}. It means that the contributions to the surface tension coming from the electrostatics is negligible. Indeed, the electrostatic part sums 0, −0.2, and +0.2 mN m^{-1} for the real and the two terms of the reciprocal space part of the Ewald summation, respectively. We also report in Figure 3a the surface tensions obtained from molecular dynamics simulations[53] for the temperature range 60−90 K. The potential used for modeling O_2 was a modified Lennard-Jones potential without any explicit consideration of the electrostatics. However, this potential gives a good agreement with experimental data.[52]

The oxygen-saturated liquid densities calculated from the two-phase simulations are predicted with an average absolute deviation of 1%, whereas the vapor densities are reproduced

Table 3. Surface Tension Values (mN m^{-1}) of the O_2 Liquid−Vapor Interface at Different Temperatures[a]

	γ_{KB}		γ_{IK}		γ_{TA}		γ_{KBZ}			
T (K)	γ_{LRC}	γ	γ_{LRC}	γ	γ_{LRC}	γ	γ_{LRC}	γ	<γ>	γ_{exp}
					O_2					
90	1.0_1	14.3_9	1.4_1	14.6_9	0.9_1	14.7_9	1.1_1	14.4_9	14.5_9	13.2
95	0.9_1	13.1_8	1.3_1	13.4_8	0.9_1	13.4_8	1.1_1	13.2_8	13.3_8	12.0
105	0.8_1	10.9_7	1.1_1	11.3_7	0.8_1	11.3_7	0.9_1	11.1_7	11.1_7	9.6
110	0.8_1	9.5_6	1.0_1	9.8_6	0.7_1	9.8_6	0.9_1	9.6_6	9.7_6	8.4
120	0.6_1	7.1_9	0.9_1	7.3_9	0.6_1	7.3_9	0.7_1	7.2_9	7.2_9	6.1
125	0.5_1	6.1_5	0.7_1	6.3_5	0.5_1	6.3_5	0.6_1	6.2_5	6.2_5	5.1
135	0.4_1	3.4_4	0.5_1	3.5_4	0.4_1	3.6_4	0.4_1	3.5_4	3.5_4	3.1
140	0.3_1	2.0_4	0.4_1	2.1_4	0.3_1	2.2_4	0.3_1	2.1_4	2.1_4	2.1

[a] Long-range corrections and the total surface tensions are given for each method. <γ> is averaged over the KB, IK, TA, and KBZ approaches. The experimental surface tensions are taken from ref 52. The long-range corrections (γ_{LRC}) and the total surface tension (γ) are given for each method. The subscripts give the accuracy of the last decimal(s); that is, 14.3_9 means 14.3 ± 0.9.

within 7% from experiments. Figure 3b compares the coexisting densities calculated from MC and GEMC methods. We observe that the two methods compare very well, leading to approximately the same absolute deviations from experiments. The critical temperature (Table 6) calculated from this phase diagram is 154.3 against 154.6 K for experiments.[50] The critical density is given with a deviation of <1% from experiments. The vapor pressures are plotted as a function of the pressure in Figure 3c and are compared by those obtained from GEMC simulations. The agreement is excellent, and the critical pressure calculated from MC simulations is 5.5 MPa against an experimental pressure of 5.0 MPa.

The average absolute deviation between the simulated and experimental surface tensions of N_2 is ∼16%. The prediction is seen to be of comparable accuracy to that carried out for the oxygen liquid−vapor interface. However, the deviations are two times larger than those observed with SO_2. The surface tensions are plotted in Figure 4a for the thermodynamic and mechanical definitions and are collected in Table 4 along with the values of the LRCs. The phase diagram of N_2 is shown in Figure 4b from GEMC, MC, and experiments. The absolute deviations calculated with the two-phase simulation are of the same order of magnitude as the ones obtained with GEMC calculations. It means that the saturated liquid densities are predicted within <1%, whereas the vapor densities are reproduced with an average deviation of 7%. The critical temperature and critical density are very well reproduced with a maximum error of 1%. The vapor pressures are reported in Figure 4c as a function of $1/T$. The agreement with experiments is excellent with an average deviation of 8 and 7% for MC and GEMC simulations, respectively. The critical pressure calculated from MC data is overestimated by 0.5 MPa, whereas it is underestimated by 0.3 MPa with GEMC.

We now turn to the case of the liquid−vapor of argon. This compound does not involve any electrostatic interactions. The surface tensions are plotted as a function of temperature in Figure 5a and are collected in Table 5. Interestingly, we observe from Figure 5 that all methods overestimate the surface tension. The absolute average deviation from experiments is ∼35% and reaches 40% with the TA method. This increase in the deviations

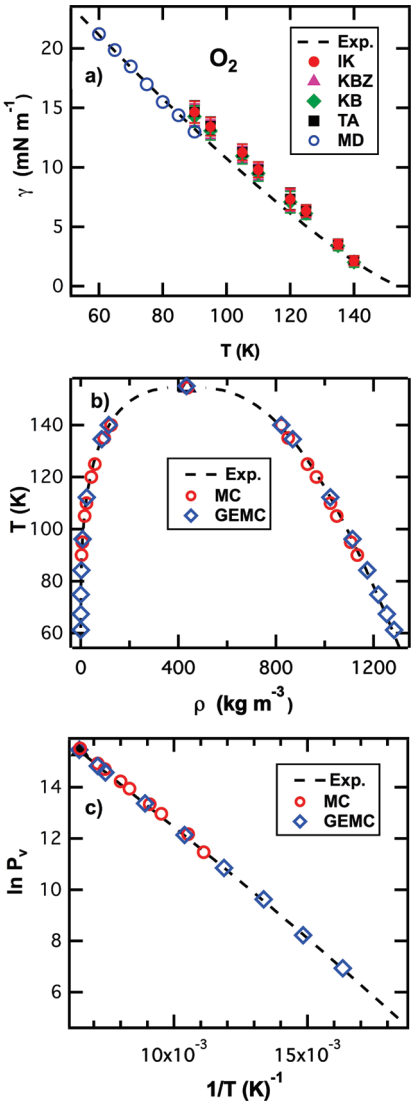

Figure 3. (a) Surface tension values of the O_2 liquid−vapor interface as a function of temperature, (b) liquid−vapor coexistence curve calculated from MC and GEMC methods, and (c) vapor pressure values as a function $1/T$. The experimental surface tensions are taken from ref 52, and the coexisting densities and vapor pressures are taken from ref 50.

with respect to experiments is quite interesting because the coexisting densities (Figure 5b) and vapor pressures (Figure 5c) do not present larger deviations from experiments than those obtained for SO_2, O_2, and N_2 compounds. The discrepancy with experiments is only for the surface tension property. The critical density and critical temperature are predicted within <1.5%, whereas the critical pressure is overestimated by 0.1 MPa by the two-phase simulation method.

The average SO_2−SO_2 interaction at 295 K is −18.7 kJ mol^{-1}, summing −11.4 and −7.3 kJ mol^{-1} for the LJ and electrostatic contributions, respectively. For N_2 (T = 75 K) and O_2 (T = 90 K), the electrostatic interactions are −0.23 and −0.03 kJ mol^{-1}, whereas the dispersion−repulsion interactions are −4.5 and −5.6 kJ mol^{-1}, respectively. For argon, the Lennard-Jones interaction is −5.2. kJ mol^{-1} at 90 K. These average energy contributions can be related to the Lennard-Jones and electrostatic contributions to the surface tension. Indeed, the

dx.doi.org/10.1021/jp204056d |J. Phys. Chem. B 2011, 115, 9421–9430

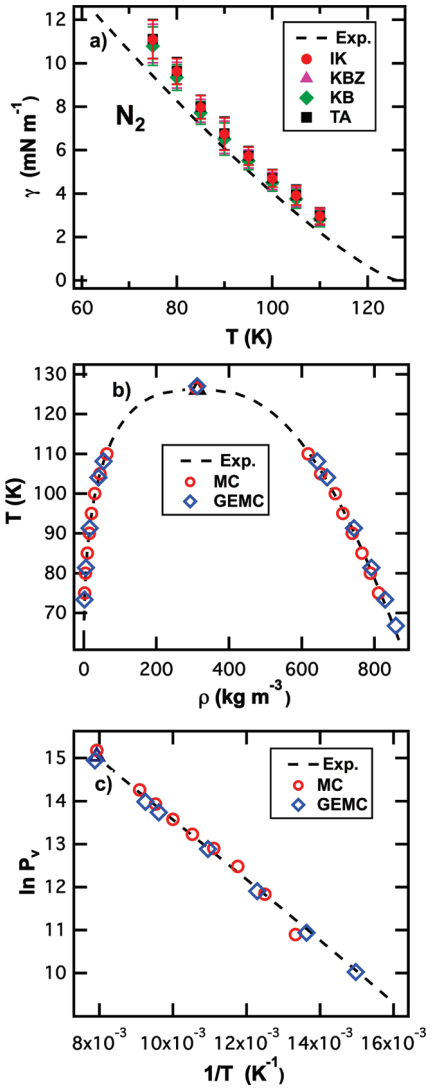

Figure 4. (a) Surface tension values of the N_2 liquid−vapor interface as a function of temperature, (b) liquid−vapor coexistence curve calculated from MC and GEMC methods, and (c) vapor pressure values as a function $1/T$. The experimental surface tensions are taken from ref 52, and the coexisting densities and vapor pressures are taken from ref 50.

electrostatic part of the surface tension decreases from 10.5 (SO_2) to 0.2 (N_2) mN m^{-1}, whereas the LJ part slightly changes from 10.5 (SO_2) to 9.6 (N_2) mN m^{-1}, indicating that the surface tensions of the O_2 and N_2 are mainly governed by Lennard-Jones interactions as for argon. This analysis of the different contributions must be related to the deviations that increase from 7% for SO_2, 15% for O_2 and N_2, and 35% for Ar.

To understand why the surface tensions of argon deviate from experiments, we plot in Figure 6a the temperature dependence of the surface tension in reduced units. The reduced properties are defined in the standard way: the temperature, $T^* = k_B T/\varepsilon$ and the surface tension $\gamma^* = \gamma\sigma^2/\varepsilon$. This representation in reduced units allows a comparison with several different literature sets of surface tensions of Lennard-Jones fluid. In Figure 6a, we plot the surface tensions of the Lennard-Jones fluid calculated by Gloor et al.[14] using the test-area method with different reduced cutoff radii of 2.5 and 5.5 σ. These values of surface tensions were not corrected by LRCs. We also add the reduced surface

Table 4. Surface Tension Values (mN m^{-1}) of the N_2 Liquid−Vapor Interface at Different Temperatures[a]

	γ_{KB}		γ_{IK}		γ_{TA}		γ_{KBZ}			
T (K)	γ_{LRC}	γ	γ_{LRC}	γ	γ_{LRC}	γ	γ_{LRC}	γ	<γ>	γ_{exp}
					N_2					
5	0.8_1	10.8_9	1.1_1	11.1_9	0.7_1	11.1_9	0.9_1	10.9_9	11.0_9	9.4
80	0.7_1	9.3_6	1.0_1	9.6_6	0.7_1	9.6_6	0.8_1	9.5_6	9.5_6	8.3
85	0.7_1	7.7_5	0.9_1	8.0_5	0.6_1	8.0_5	0.8_1	7.8_5	7.9_5	7.2
90	0.6_1	6.5_7	0.8_1	6.7_7	0.6_1	6.8_8	0.7_1	6.6_7	6.7_8	6.1
95	0.5_1	5.5_4	0.7_1	5.7_4	0.5_1	5.7_4	0.6_1	5.6_4	5.6_4	5.0
100	0.5_1	4.5_4	0.7_1	4.7_4	0.5_1	4.7_4	0.6_1	4.6_4	4.6_4	4.1
105	0.4_1	3.8_4	0.5_1	3.9_4	0.4_1	3.9_4	0.5_1	3.8_4	3.9_4	3.1
110	0.3_1	2.8_4	0.4_1	3.0_4	0.3_1	3.0_4	0.4_1	2.9_4	2.9_4	2.2

[a] Long-range corrections and the total surface tensions are given for each method. <γ> is averaged over the KB, IK, TA, and KBZ approaches. The experimental surface tensions are taken from ref 52. The long-range corrections (γ_{LRC}) and the total surface tension (γ) are given for each method. The subscripts give the accuracy of the last decimal(s); that is, 11.9_9 means 11.9 ± 0.9.

tensions[54] of Janecek calculated with a special treatment of the LRCs during the course of the simulation. We report the surface tensions calculated by Errington using the technique of the finite-size scaling framework of Binder[55] and the grand canonical ensemble to calculate the free-energy barrier between the liquid and vapor phases.[56] The surface tensions of Errington have also been corrected by the LRC contribution. In addition, the simulated surface tensions of methane[12] and argon of this work are scaled in reduced units. We only use the surface tensions that are calculated from the IK definition and corrected by long-range contributions. The experimental surface tensions of methane and argon are represented in Figure 6a by dotted points in reduced units. The deviations from experiments cannot be attributed to the system-size effects because the interfacial areas used here and the box size along the normal to the interface satisfy the recommendations given by Biscay et al.[6] First, we observe that the reduced surface tensions of Gloor et al. (open circles and diamonds) are cutoff-dependent because no LRCs were applied in these calculations. When specific LRCs are introduced in the calculation, the surface tensions (full symbols in Figure 6a) are consistent with each other. When the calculation of the surface tension is carried out with a larger cutoff of 5.5 σ (diamond), the simulated values exhibit the smallest deviations from experiments. However, these values should be modified by a LRC term, leading to a more accentuated overestimation. Figure 6b reports the reduced surface tensions calculated with three different cutoff radii (r_c = 3.5, 4.4, and 5.4 σ), where the value of 5.4 σ is large enough to approach the full LJ potential results.[6,7] We check that the corrected surface tensions compare very well with the values calculated with the largest cutoff radius. This shows the need of using LRCs for the surface tension to avoid the use of too-large cutoffs. We also observe a discrepancy between intrinsic surface tensions (without any added LRCs) and experiments, even for a cutoff of 5.4 σ.

The overestimation of the surface tension of argon is not due to the system-size effects, the LRCs, and the cutoff value. It has been already shown in the past for argon[57] and has been attributed by the use of the Lennard-Jones potential, which does not represent an accurate potential for argon. The modeling of

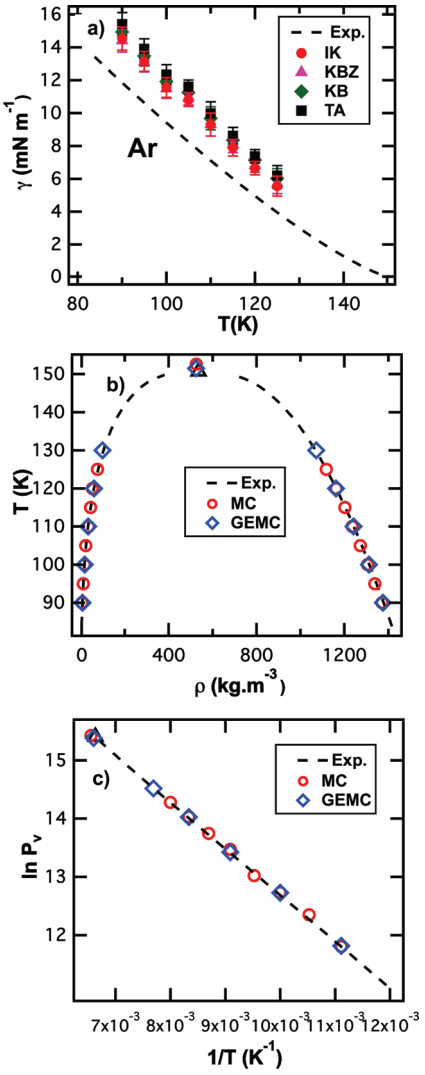

Figure 5. (a) Surface tension values of the Ar liquid−vapor interface as a function of temperature, (b) liquid−vapor coexistence curve calculated from MC and GEMC methods, and (c) vapor pressure values as a function $1/T$. The experimental surface tensions are taken from ref 52, and the coexisting densities and vapor pressures are taken from ref 50.

three or higher-body interactions could be an alternative for the prediction of the surface tension of argon. The good agreement between the experimental and simulated coexisting densities is then only due to the fact that the parameters of the LJ potential have been optimized over the liquid densities. However, the prediction fails for properties that do not belong to the adjustment database.

CONCLUSIONS

The results in this Article indicate that two-phase simulations of studying two phases in coexistence give vapor and liquid densities, vapor pressure, critical temperature, critical density, and critical pressure in excellent agreement with those calculated with the GEMC methods using the same potential. The deviations from experiments are of the same order of magnitude for the two techniques, indicating that the system sizes used here allow us to obtain well-developed bulk liquid and vapor phases.

Table 5. Surface Tension Values (mN m^{-1}) of the Ar Liquid−Vapor Interface at Different Temperatures[a]

	γ_{KB}		γ_{IK}		γ_{TA}		γ_{KBZ}			
T (K)	γ_{LRC}	γ	γ_{LRC}	γ	γ_{LRC}	γ	γ_{LRC}	γ	<γ>	γ_{exp}
					Ar					
90	3.4_1	14.9_7	3.1_1	14.5_7	3.0_1	15.4_7	2.9_1	14.4_7	15.0_7	11.9
95	3.2_1	13.5_6	2.8_1	13.1_6	2.8_1	13.9_6	2.8_1	13.1_6	13.5_6	10.6
100	3.0_1	11.9_6	2.7_1	11.6_6	2.6_1	12.3_6	2.6_1	11.5_6	11.9_6	9.4
105	2.8_1	11.3_4	2.4_1	10.8_4	2.5_1	11.6_4	2.4_1	10.9_4	11.2_4	8.2
110	2.6_1	9.7_7	2.2_1	9.3_7	2.3_1	10.0_7	2.2_1	9.3_7	9.7_7	7.1
115	2.4_1	8.4_5	2.0_1	7.9_5	2.1_1	8.6_5	2.1_1	8.1_5	8.3_5	6.0
120	2.2_1	7.1_4	1.7_1	6.6_4	2.0_1	7.4_4	1.9_1	6.8_4	7.1_4	5.0
125	1.9_1	6.0_6	1.5_1	5.6_6	1.7_1	6.2_6	1.6_1	5.7_6	5.9_6	4.0

[a] Long-range corrections and the total surface tensions are given for each method. <γ> is averaged over the KB, IK, TA, and KBZ approaches. The experimental surface tensions are taken from ref 52. The long-range corrections (γ_{LRC}) and the total surface tension (γ) are given for each method. The subscripts give the accuracy of the last decimal(s); that is, 15.0_7 means 15.0 ± 07.

Table 6. Critical Temperatures, Critical Densities and Critical Pressures Calculated from Data Obtained by MC and GEMC Simulations[36,38 a]

T_c (K)			ρ_c (kg m^{-3})			P_c (MPa)		
MC	GEMC	exp	MC	GEMC	exp	MC	GEMC	exp
				SO_2				
429.4	432.5	430.6	539.8	529.7	525.0	8.5	8.5	7.9
				O_2				
154.3	155.0	154.6	437.6	433.2	436.1	5.5	5.2	5.0
				N_2				
126.2	127.0	126.2	309.6	312.4	313.3	3.9	3.1	3.4
				Ar				
152.6	151.5	150.7	526.2	525.0	535.6	5.0	4.8	4.9

[a] Eperimental properties[50] are given for comparison.

The aim of this Article was to predict the dependence of the surface tension of SO_2, O_2, N_2, and Ar with temperature. It represents a genuine test of the transferability of the potentials because the parameters of these potentials were developed only on bulk and critical properties.

The force field used here for SO_2 can accurately reproduce the experimental surface tension over the temperature range 295−400 K. All definitions of the surface tension give similar results within the error bars of the calculation. The intermolecular interactions in the O_2 and N_2 compounds are mainly governed by dispersive−repulsive interactions. The electrostatic interactions in these compounds are much smaller than those in SO_2 and can be considered to be insignificant. The prediction of the surface tension of these compounds shows larger deviations (two times larger than those obtained for SO_2). Nevertheless, the reproduction of the temperature dependence of the surface tension for O_2 and N_2 is reasonable with an average deviation of 15%. The coexisting densities and the critical properties (density,

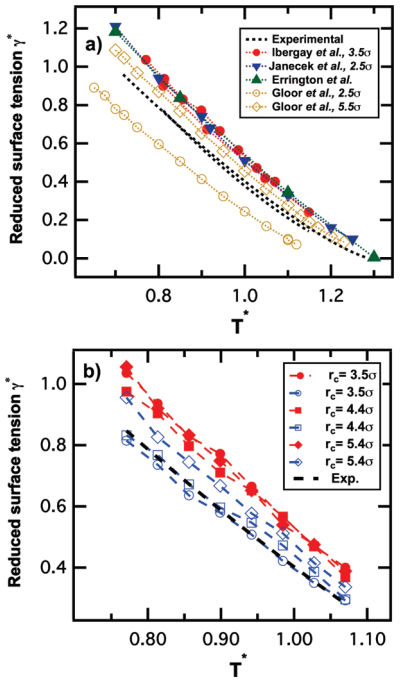

Figure 6. (a) Reduced γ^* surface tensions as a function of the reduced temperature calculated from different methodologies. The dotted and dashed lines correspond to the experimental surface tensions of methane[49] and argon[52] scaled in reduced units. The surface tensions of argon result from this work; those for methane are from ref 12. The data of the surface tensions of the Lennard-Jones fluid are taken from the works of Gloor et al. (ref 14) with two different values of cutoff (2.5 and 3.5 σ), of Janecek (ref 54), and of Errington et al. (ref 56). (b) Intrinsic (open symbols) and total (filled symbols) surface tensions calculated with the IK definition using three different cutoff values. The dotted line corresponds to the experimental surface tensions.[52]

temperature, and pressure) of O_2 and N_2 are estimated with the same accuracy as those of SO_2 and are in very good agreement with the corresponding experimental ones.

The calculation of the surface tension of argon reveals that the parameters of the Lennard-Jones pair potential developed from coexisting densities, and critical points give rise to major deviations in the prediction of the surface tension for compounds only governed by dispersion−repulsion interactions. This has been shown by representing the surface tensions of the Lennard-Jones fluid in reduced units. The comparison with various surface tensions of the literature has shown that the values calculated here for argon are in line with existing reduced surface tensions once the LRCs are applied to the intrinsic part. The use of LRCs leads to overestimate the surface tension in fluids for which the Lennard-Jones interactions are predominant. This is not the case in compounds with significant electrostatic interactions, as shown for SO_2. One solution would be to introduce three or higher-body interactions in the model of argon.

■ CONVERGENCE OF THE SURFACE TENSION IN EACH BLOCK-AVERAGE

Figure A-1 shows that the number of cycles and the number of steps per cycles is large enough to respect the convergence of the surface tension within each block.

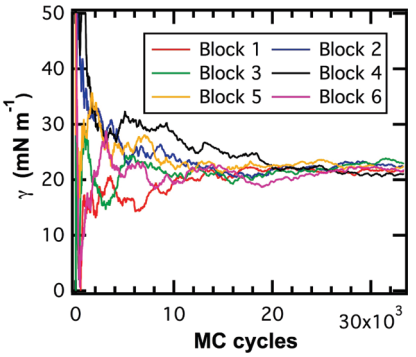

Figure A-1. Convergence of the average surface tension as a function of the number of cycles in each block average. The surface tension is calculated using the IK definition for the liquid−vapor interface of SO_2 at 295 K.

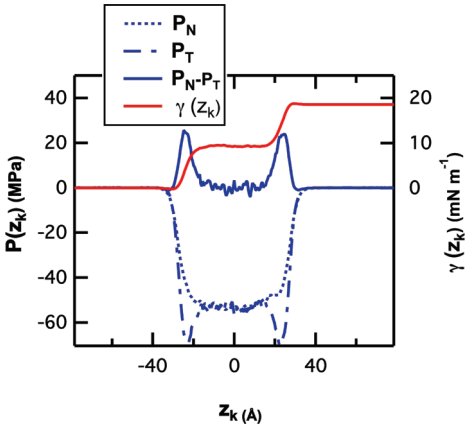

Figure B-1. Profiles of the tangential $p_T(z_k)$ and normal $p_N(z_k)$ components of the configurational part of the pressure tensor calculated in the liquid−vapor interface of SO_2 at 295 K. The profile of $p_N(z_k) - p_T(z_k)$ and of its integral $\gamma(z)$ is also given for completeness.

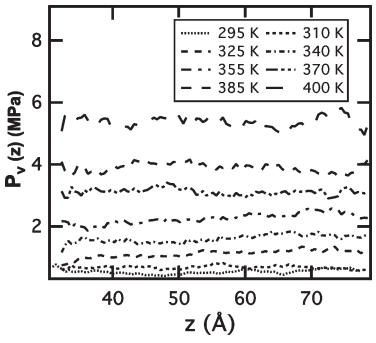

Figure B-2. Profiles of the normal component of the pressure tensor calculated using the IK definition in the vapor phase of SO_2.

■ PROFILES OF THE NORMAL COMPONENTS OF THE PRESSURE TENSOR IN THE VAPOR PHASE

The profile of the difference $(p_N(z_k) - p_T(z_k)$ shown in Figure B-1presents two positive peaks at the interfacial regions, as expected from a two-phase system. The profile of the normal component of the pressure tensor shown in Figure B-2sums the Lennard-Jones, electrostatic, and long range corrections parts of

dx.doi.org/10.1021/jp204056d |J. Phys. Chem. B 2011, 115, 9421–9430

the pressure. The reader is redirected to refs 25, 28, and 31 for a review about the calculation of these different terms.

AUTHOR INFORMATION

Corresponding Author

*E-mail: Patrice.Malfreyt@univ-bpclermont.fr.

REFERENCES

(1) *IPPC Special Report on Carbon Dioxide Capture and Storage*; Cambridge University Press: Cambridge, U.K., 2005.
(2) Anheden, M.; Andersson, A.; Bernstone, C.; Eriksson, S.; Yan, J.; Liljemark, S.; Wall, C. In *CO_2 Quality Requirements for a System with CO_2 Capture, Transport and Storage*, Proceedings of GHGT-7, Vol. II; Vancouver, 2004; pp 2559−2563.
(3) Orea, P.; Lopez-Lemus, J.; Alejandre, J. *J. Chem. Phys.* **2005**, *123*, 114702.
(4) Gonzalez-Melchor, M.; Orea, P.; Lopez-Lemus, J.; Bresme, F.; Alejandre, J. *J. Chem. Phys.* **2005**, *122*, 094503.
(5) Errington, J. R.; Kofke, D. A. *J. Chem. Phys.* **2007**, *127*, 174709.
(6) Biscay, F.; Ghoufi, A.; Goujon, F.; Lachet, V.; Malfreyt, P. *J. Chem. Phys.* **2009**, *130*, 184710.
(7) Trokhymchuk, A.; Alejandre, J. *J. Chem. Phys.* **1999**, *111*, 8510.
(8) Lopez-Lemus, J.; Alejandre, J. *Mol. Phys.* **2002**, *100*, 2983.
(9) Goujon, F.; Malfreyt, P.; Boutin, A.; Fuchs, A. H. *J. Chem. Phys.* **2002**, *116*, 8106.
(10) Grosfils, P.; Lutsko, J. F. *J. Chem. Phys.* **2009**, *130*, 054703.
(11) Goujon, F.; Malfreyt, P.; Simon, J. M.; Boutin, A.; Rousseau, B.; Fuchs, A. H. *J. Chem. Phys.* **2004**, *121*, 12559.
(12) Ibergay, C.; Ghoufi, A.; Goujon, F.; Ungerer, P.; Boutin, A.; Rousseau, B.; Malfreyt, P. *Phys. Rev. E* **2007**, *75*, 051602.
(13) Goujon, F.; Bonal, C.; Malfreyt, P. *Mol. Simulat.* **2009**, *35*, 538.
(14) Gloor, G. J.; Jackson, G.; Blas, F. J.; de Miguel, E. *J. Chem. Phys.* **2005**, *123*, 134703.
(15) Ghoufi, A.; Goujon, F.; Lachet, V.; Malfreyt, P. *Phys. Rev. E* **2008**, *77*, 031601.
(16) Guo, M.; Lu, B. C. Y. *J. Chem. Phys.* **1997**, *106*, 3688.
(17) Shen, V. K.; Mountain, R. D.; Errington, J. R. *J. Phys. Chem. B* **2007**, *111*, 6198.
(18) Goujon, F.; Malfreyt, P.; Boutin, A.; Fuchs, A. H. *Mol. Simul.* **2001**, *27*, 99.
(19) Biscay, F.; Ghoufi, A.; Goujon, F.; Lachet, V.; Malfreyt, P. *J. Phys. Chem. B* **2008**, *112*, 13885.
(20) Janecek, J.; Krienke, H.; Schmeer, G. *Condens. Matter Phys.* **2007**, *10*, 415.
(21) Nieto-Draghi, C.; Bonnaud, P.; Ungerer, P. *J. Phys. Chem. C* **2007**, *111*, 15686.
(22) Biscay, F.; Ghoufi, A.; Lachet, V.; Malfreyt, P. *Phys. Chem. Chem. Phys.* **2009**, *111*, 6132.
(23) Alejandre, J.; Tildesley, D. J.; Chapela, G. A. *J. Chem. Phys.* **1995**, *102*, 4574.
(24) Vega, C.; de Miguel, E. *J. Chem. Phys.* **2007**, *126*, 154707.
(25) Ghoufi, A.; Goujon, F.; Lachet, V.; Malfreyt, P. *J. Chem. Phys.* **2008**, *128*, 154716.
(26) Ghoufi, A.; Goujon, F.; Lachet, V.; Malfreyt, P. *J. Chem. Phys.* **2008**, *128*, 154718.
(27) Biscay, F.; Ghoufi, A.; Lachet, V.; Malfreyt, P. *J. Phys. Chem. C* **2011**, *115*, 8670.
(28) Biscay, F.; Ghoufi, A.; Lachet, V.; Malfreyt, P. *J. Chem. Phys.* **2009**, *131*, 124707.
(29) Ghoufi, A.; Malfreyt, P. *Phys. Chem. Chem. Phys.* **2010**, *12*, 5203.
(30) Biscay, F.; Ghoufi, A.; Malfreyt, P. *Phys. Chem. Chem. Phys.* **2011**, *13*, 11308.
(31) Biscay, F.; Ghoufi, A.; Lachet, V.; Malfreyt, P. *J. Phys. Chem. B* **2009**, *113*, 14277.
(32) Biscay, F.; Ghoufi, A.; Malfreyt, P. *J. Chem. Phys.* **2011**, *134*, 044709.
(33) Abascal, J. L. F.; Vega, C. *J. Chem. Phys.* **2005**, *123*, 234505.
(34) Ferrando, N.; Lachet, V.; Teuler, J. M.; Boutin, A. *J. Phys. Chem. B* **2009**, *113*, 5985.
(35) Delhommelle, J. Ph.D. Thesis, Université de Paris XI, Orsay, France, 2000.
(36) Vrabec, J.; Stoll, J.; Hasse, H. *J. Phys. Chem. B* **2001**, *105*, 12126.
(37) Boutard, Y.; Ungerer, P.; Teuler, J. M.; Ahunbay, M. G.; Sabater, S. F.; Perez-Pellitero, J.; Mackie, A. D.; Bourasseau, E. *Fluid Phase Equilib.* **2005**, *236*, 25.
(38) ElAhmar, E.; Creton, B.; Valtz, A.; Coquelet, C.; Lachet, V.; Richon, D.; Ungerer, P. *Fluid Phase Equilib.* **2011**, *304*, 21.
(39) Panagiotopoulos, A. Z. *Mol. Phys.* **1987**, *61*, 813.
(40) Panagiotopoulos, A. Z.; Quirke, N.; Stapleton, M.; Tildesley, D. J. *Mol. Phys.* **1988**, *63*, 527.
(41) Allen, M. P.; Tildesley, D. J. *Computer Simulations of Liquids*; Clarendon Press: Oxford, U.K., 1989.
(42) Smith, E. R. *Proc. R. Soc. London, Ser. A* **1981**, *375*, 475.
(43) Heyes, D. M. *Phys. Rev. B* **1994**, *49*, 755.
(44) Rowlinson, J. S.; Widom, B. *Molecular Theory of Capillarity*; Clarendon Press: Oxford, U.K., 1982.
(45) Kirkwood, J. G.; Buff, F. P. *J. Chem. Phys.* **1949**, *17*, 338.
(46) Irving, J. H.; Kirkwood, J. G. *J. Chem. Phys.* **1950**, *18*, 817.
(47) Walton, J. P. R. B.; Tildesley, D. J.; Rowlinson, J. S.; Henderson, J. R. *Mol. Phys.* **1983**, *48*, 1357.
(48) Walton, J. P. R. B.; Gubbins, K. E. *Mol. Phys.* **1985**, *55*, 679.
(49) Somayajulu, G. R. *Int. J. Thermophys.* **1988**, *9*, 559.
(50) Lemmon, E. W.; McLinden, M. O.; Friend, D. G. *Thermophysical Properties of Fluid Systems*; in NIST Chemistry WebBook, NIST Standard Reference Database Number 69; Linstrom, P. J., Mallard, W. G., Eds.; National Institute of Standards and Technology, Gaithersburg, MD, 2005. http://webbook.nist.gov (accessed Jan 5, 2011).
(51) Rowlinson, J.; Swinton, F. *Liquid and Liquid Mixtures*, 3rd ed.; Butterworths: London, 1982.
(52) Lemmon, E. W.; Penoncello, S. G. *Adv. Cryog. Eng.* **1994**, *39*, 1927.
(53) Bembenek, S. D. *J. Chem. Phys.* **2006**, *124*, 014709.
(54) Janecek, J. *J. Phys. Chem. B* **2006**, *110*, 6264.
(55) Binder, K. *Phys. Rev. A* **1982**, *25*, 1699.
(56) Errington, J. R. *Phys. Rev. E* **2003**, *67*, 012102.
(57) Miyazaki, J.; Barker, J. A.; Pound, G. M. *J. Chem. Phys.* **1976**, *64*, 3364.